Polímeros
ISSN 1678-5169 (Online)

https://doi.org/10.1590/0104-1428.20240094

ORIGINAL ARTICLES

Gold nanoparticles based on polysaccharide from *Amburana cearensis* for organic dyes degradation

Eziel Cardoso da Silva[1], Emanuel Airton de Oliveira Farias[1,2], Thais Danyelle Santos Araújo[2], Alyne Rodrigues Araújo[2], Geanderson Emilio de Almeida[1], Lívio César Cunha Nunes[3] and Carla Eiras[1]*

[1]Laboratório de Pesquisa e Desenvolvimento de Novos Materiais e Sistemas Sensores – MATSENS, Universidade Federal do Piauí – UFPI, Teresina, PI, Brasil

[2]Universidade Estadual Vale do Acaraú – UVA, Camocim, CE, Brasil

[3]Laboratório de Inovação Tecnológica e Empreendedorismo – LITE, Universidade Federal do Piauí – UFPI , Teresina, PI, Brasil

**eirasc@ufpi.edu.br*

Abstract

Gold nanoparticles (AuNPs) were prepared by green synthesis using the gum extracted from *Amburana cearensis* (GAmb) exudate. The influence of polysaccharide concentration, precursor salt ($HAuCl_4$), temperature, pH, and reaction time on the final properties of the AuNPs-GAmb was evaluated. The UV-VIS spectrum of the AuNPs-GAmb showed an absorption band in the region of 524 nm, characteristic of spherical nanostructures, and the synthesis conditions strongly influenced the average diameter of these nanoparticles. The optimized AuNPs-GAmb presented a high colloidal stability and spherical shape with an average diameter of 13.22 ± 1.86 nm (when measured by Atomic Force Microscopy -AFM). Later, the catalytic activity of AuNPs-GAmb was evaluated in the degradation of toxic dyes such as toluidine blue (TB), methylene blue (MB), and methyl orange (MO), which were degraded in less than 11 minutes. Thus, the AuNPs-GAmb obtained in this work are eco-friendly and have a high potential for applications in biotechnology.

Keywords: *tree exudate, green technologies, nanotechnology, environmental remediation.*

Data Availability: All data supporting the findings of this study are included in this article and its supplementary materials.

How to cite: Silva, E. C., Farias, E. A. O., Araújo, T. D. S., Araújo, A. R., Almeida, G. E., Nunes, L. C. C., & Eiras, C. (2025). Gold nanoparticles based on polysaccharide from Amburana cearensis for organic dyes degradation. *Polímeros: Ciência e Tecnologia, 35*(3), e20250029. https://doi.org/10.1590/0104-1428.20240094

1. Introduction

Growing environmental awareness has directed efforts toward the search for an approach called "green chemistry" or "sustainable chemistry," which aims to eliminate harmful reagents in the development of new products[1].

Gold nanoparticles (AuNPs) are among the most studied nanomaterials due to their excellent properties: high stability, low toxicity, and biocompatibility. Different strategies have been proposed for the synthesis of AuNPs, from the most conventional ones (using reducing agents) to strategies such as photochemical and radiolytic synthesis, among others. However, the green synthesis approach stands out due to the use of natural molecules such as enzymes, amino acids, proteins, and polysaccharides[2].

Considering that gum or polysaccharides extracted from plant species, such as Karaya gum (Sterculia urens) and Acacia gum (*Acacia seyal*), have been used as reducing and stabilizing agents in the synthesis of AuNPs, the gum extracted from the trunk exudate of the *Amburana cearensis* AC Smith (GAmb), emerges as a new alternative in the synthesis of these nanoparticles. *A. cearensis* is a tree that occurs naturally in Brazil's northeast, southeast, and central-west states. It can also be found in other South American countries, such as Argentina, Paraguay, and Bolivia[3].

Among the applications proposed for AuNPs, their function as a catalyst agent during reducing toxic dyes stands out. Thus, green products such as the AuNPs-GAmb proposed in this work may deactivate dyes such as methyl orange, toluidine blue, and methylene blue.

The methyl orange or MO ($C_{14}H_{14}N_3NaO_3S$) is an example of a highly toxic, mutagenic, non-biodegradable, and carcinogenic, widely used in various industrial sectors[4]. Another well-known dye is toluidine blue or TB ($C_{15}H_{16}N_3SCl$), which is commonly used in the textile industry. TB has been reported to be mutagenic and may irritate animals' skin or affect their genomes[5]. Methylene blue or MB ($C_{16}H_{18}ClN_3S$) is a non-biodegradable cationic dye used for decades in paper, rubber, and plastic industries[6].

Although sodium borohydride ($NaBH_4$) is considered a potent reducing agent, including used in the synthesis of Pt, Ag, and Au nanoparticles, it does not favor the degradation

of these dyes. On the other hand, recent approaches that have been tested include the addition of catalysts, such as metal nanoparticles, preferably from green synthesis routes, to enhance the degradation[7].

Thus, this study aimed to synthesize gold nanoparticles using *A. cearensis* polysaccharide (AuNPs-GAmb) as a reducing and stabilizing agent for subsequent application in degrading toxic dyes, such as methyl orange, toluidine blue, and methylene blue.

2. Materials and Methods

2.1 Isolation and Purification of A. cearensis gum (GAmb)

The methodology used to isolate and purify the polysaccharide from *A. cearensis* followed that of Farias et al.[8].

2.2 Synthesis of gold nanoparticles (AuNPs-GAmb)

The methodology selected for synthesizing AuNPs-GAmb was adapted from the study by Melo et al.[9]. In an Erlenmeyer flask, 10.0 mL of GAmb solution was added, which was heated and stirred (300 rpm). After, 10.0 mL of tetrachloroauric (III) acid trihydrate ($HAuCl_4$ $3.H_2O$) (Sigma-Aldrich) solution was added. During synthesis, the following parameters were optimized: the concentrations of GAmb variated between 0.1, 0.2, or 0.3% (w/v), and $HAuCl_4$ $3.H_2O$ variated between 0.1, 0.2, or 0.3 mM. A volume of 10 mL was maintained for GAmb and $HAuCl_4$ $3.H_2O$ in all experiments (total volume = 20 mL). The influence of temperature (varying between 80, 90, or 100 ºC), pH (ranging between 2.5, 3.0, and 3.5), and synthesis time (30, 60, and 120 min) were also evaluated. Table 1 summarizes the synthesis parameters.

2.3 Characterizations of AuNPs-GAmb

Before characterization, the AuNPs-GAmb were subjected to four centrifugation processes at 4,000 rpm for 20 min, based on the study by Silva[10].

UV-Vis analyses were performed using a Shimadzu UV mini 1240 spectrophotometer in the 400-800 nm wavelength range, using a quartz cuvette containing 1.0 mL of AuNPs-GAmb. Infrared spectroscopy (FTIR) measurements were performed on a Shimadzu IRAffinity-1 spectrophotometer in the 400-4000 cm^{-1} range. DLS (Dynamic Light Scattering) measurements were performed on a Malvern Zetasizer Nano ZS90. AFM analyses were performed in TT-AFM equipment (AFM Workshop, USA), in intermittent contact (vibratory) mode (with a resolution of 512 × 512 pixels), using TAP300-G silicon probes (Ted Pella, USA) and a resonance frequency of approximately 240 kHz. The images obtained were analyzed in the Gwyddion 2.61 software.

2.4 Catalytic activity

After optimizing the synthesis parameters, a study was conducted to investigate the catalytic effect of AuNPs-GAmb on the degradation of methylene blue (MB), toluidine blue (TB), and methyl orange (MO) dyes[11-13]. The effectiveness of the $NaBH_4$ + AuNPs-GAmb system in degrading the dyes (MB, TB, and MO) was estimated using Equation 1:

$$\%degradation = \left\{ \left(A0 - At \right) / A0 \right\} \times 100 \quad (1)$$

Where:

A0 and At are the absorbance at 0 and t minutes, respectively.

2.5 ABTS radical scavenging assay

The antioxidant activity of AuNPs-GAmb was determined by the ABTS method ((2,2′-Azino-bis-(3-ethylbenzothiazoline-6-sulfonic acid), diammonium salt, from the study adapted from Gião et al.[14].

3. Results and Discussions

3.1 Gold nanoparticles reduced and stabilized with GAmb

3.1.1 Synthesis mechanism

The synthesis of AuNPs-GAmb starts from an aqueous solution of gold and a reducing and stabilizer agent (GAmb) solution. The structure of GAmb and the synthesis mechanism

Table 1. AuNPs-GAmb obtained under different synthesis conditions.

	GAmb conc. (%)	$HAuCl_4$ conc (mM)	Temp. (ºC)	pH	Synthesis time (min)	Polydispersity index (PDI)	Diameter (nm) measured by DLS	Zeta potential (mV)
Study of GAmb Conc. (%)	**0.10**	0.20	100	3.50	30	0.53 ± 0.02	45.93 ± 1.60	-22.00 ± 0.64
	0.20	0.20	100	3.50	30	**0.47 ± 0.05**	**53.86 ± 1.11**	**-25.13 ± 1.15**
	0.30	0.20	100	3.50	30	0.72 ± 0.03	94.82 ± 1.19	-29.16 ± 2.56
Study of HAuCl4 Conc. (mM)	0.20	**0.10**	100	3.50	30	0.59 ± 0.05	116.7 ± 8.20	-22.73 ± 0.26
	0.20	**0.20**	100	3.50	30	0.47 ± 0.05	82.82 ± 4.79	-25.13 ± 1.15
	0.20	**0.30**	100	3.50	30	**0.61 ± 0.01**	**52.55 ± 2.17**	**-21.73 ± 0.59**
Study of Temperature Variation	0.20	0.30	**80**	3.50	30	0.96 ± 0.03	19.94 ± 1.07	-17.23 ± 1.12
	0.20	0.30	**90**	3.50	30	0.62 ± 0.02	32.44 ± 0.84	-19.50 ± 0.48
	0.20	0.30	**100**	3.50	30	**0.61 ± 0.01**	**52.55 ± 2.17**	**-21.73 ± 0.59**
Study of pH Variation	0.20	0.30	100	**2.50**	30	0.42 ± 0.03	126.30 ± 4.1	-5.570 ± 0.81
	0.20	0.30	100	**3.00**	30	0.41 ± 0.05	99.47 ± 3.69	-8.250 ± 0.81
	0.20	0.30	100	**3.50**	30	**0.61 ± 0.01**	**52.55 ± 2.17**	**-21.73 ± 0.59**
Influence of Synthesis Time	0.20	0.30	100	3.50	**30**	0.61 ± 0.01	52.55 ± 2.17	-21.73 ± 0.59
	0.20	0.30	100	3.50	**60**	**0.65 ± 0.11**	**32.39 ± 0.80**	**-20.40 ± 0.71**
	0.20	0.30	100	3.50	**120**	0.66 ± 0.03	26.50 ± 0.78	-18.80 ± 0.63

of AuNPs-GAmb are shown in Figure 1. GAmb is a polyhydroxylated biopolymer consisting of a β-D-Galactopyran backbone linked by glycosidic bonds (1→3). At the same time, the side chains exhibit β-Galactopyranose (1→6) and α-L-Arabinofuranoside (1→3,6) monomers[15]. Many hydroxyl groups and the reducing ends of GAmb act as active reaction centers to facilitate the reduction of Au^{3+} to Au^{0}. The synthesis process goes through the steps of reduction, nucleation, and stabilization, giving rise to AuNPs-GAmb.

3.1.2 Optimization of synthesis parameters

In all syntheses performed, the formation of AuNPs-GAmb was evidenced by the change in color of the reaction medium, from pale yellow (characteristic of the $HAuCl_4$ - gold salt solution) to red, resulting from the excitation of the surface plasmon resonance (SPR) of AuNPs-GAmb. Thus, during this study stage, the synthesis was optimized to search for AuNPs-GAmb that exhibited the best properties. Therefore, the synthesis parameters (precursor concentration, temperature, pH, and reaction time) were monitored by UV-visible (UV-VIS) spectroscopy and DLS techniques.

Figure 2A shows the UV-VIS spectra obtained in the synthesis of AuNPs-GAmb in which the polysaccharide concentrations were varied at 0.1, 0.2, and 0.3% (w/v). Here, all syntheses were performed in triplicates, maintaining the pH of the reaction medium at 3.5, the concentration of $HAuCl_4$ at 0.2 mM, the reaction temperature at 100 °C, and the synthesis time at 30 minutes. Figure 2B shows the spectra obtained from the average of these measurements.

From the spectra obtained, it can be observed that with the increase in the concentration of GAmb in the reaction medium, the SPR band moved to a region of shorter wavelength with an increase in the absorbance intensity. This behavior shows a tendency of growth in the average diameter of these nanoparticles, corroborating the data obtained by DLS presented in Table 1. This can be explained by an aggregation of nanoparticles, mainly when using 0.3% GAmb. Thus, using GAmb at 0.1, 0.2, or 0.3% made it possible to obtain nanoparticles with diameters varying respectively between 45.93, 53.86, and 94.82 nm. When GAmb was used at 0.3%, the PDI was 0.726, which characterizes a polydisperse system[16].

The AuNPs-GAmb obtained at 0.2% of the polysaccharide presented a slightly lower PDI (0.477 ± 0.05) than that obtained for the AuNPs at 0.1% of GAmb (0.530 ± 0.02), Table 1. In addition, the concentration of 0.2%, when compared to 0.1% of GAmb, ensures greater availability of reducing groups such as carbonyl and hydroxyl present in the polysaccharide, which can favor synthesis. According to Chopra et al.[17], the increase in the concentrations of reducers results in a more significant formation of AuNPs. Therefore, the concentration at 0.2% of GAmb was considered the most suitable and kept constant in the following steps of optimization of the synthesis parameters.

A study with locust bean gum (*Ceratonia siliqua*) demonstrated that the efficiency of AuNPs formation increased with the increase of gum concentration (keeping the $HAuCl_4$ concentration constant). On the other hand, this correlation was not observed when sodium citrate was used as a reduction agent instead of gum during these AuNPs synthesis[18,19].

Subsequently, the influence of the $HAuCl_4$ concentration (0.1, 0.2, or 0.3 mM) on the synthesis of AuNPs-GAmb was evaluated.

Figure 2C and 2D show the spectra absorption obtained in triplicates and its respective averages for AuNPs-GAmb obtained under different concentrations of $HAuCl_4$. The syntheses with $HAuCl_4$ at 0.2 mM recorded the lowest absorbance values at 530 nm, indicating the lowest concentration of nanoparticles in the colloidal suspension. On the other hand, the highest absorbance values were presented in the synthesis using 0.3 mM $HAuCl_4$, indicating more nanoparticles were obtained.

Another important observation is that the increase in the concentration of $HAuCl_4$ promoted a decrease in AuNPs-GAmb diameter, which was 116.7 nm for $HAuCl_4$ at 0.1 mM, 82.8 nm for $HAuCl_4$ at 0.2 mM, and 52.6 nm for $HAuCl_4$ at 0.3 mM (Table 1).

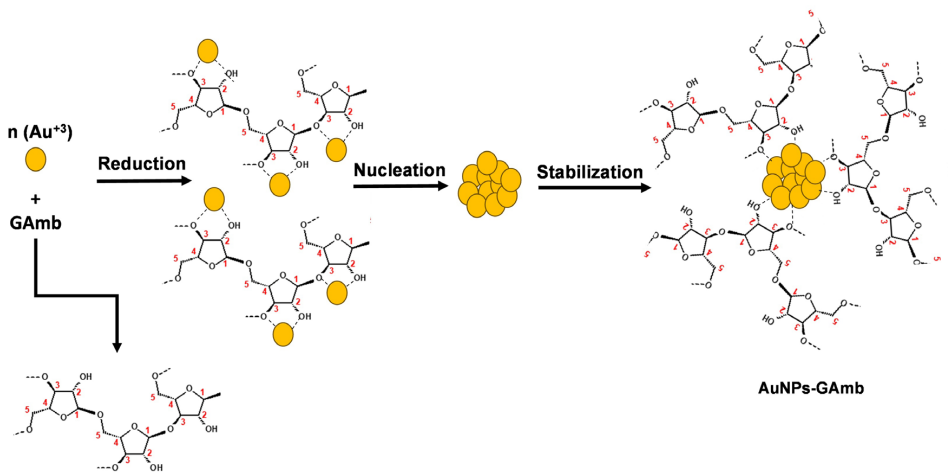

Figure 1. Mechanism for the formation of AuNPs-GAmb.

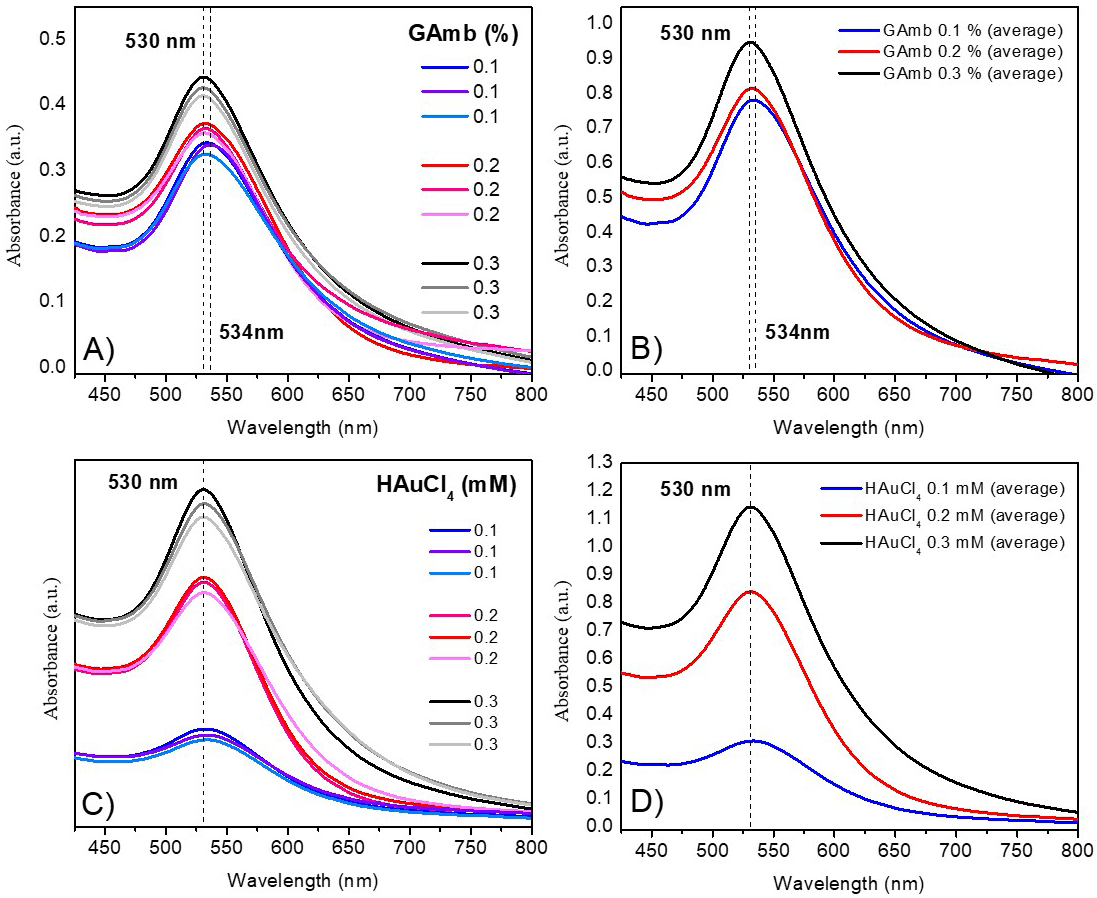

Figure 2. UV-Vis spectra (A) were obtained in triplicates while studying the influence of the GAmb concentration (0.1, 0.2, or 0.3%) and (B) on the average of these triplicates. (C) UV-Vis spectra obtained in triplicates during the study of the influence of $HAuCl_4$ concentration (0.1, 0.2, and 0.3 mM) and (D) average of these triplicates. Constant parameters: pH = 3.5, temperature =100 °C and synthesis time = 30 min.

According to the literature[20], this occurs due to an increase in the concentration of the anion $[AuCl_4]^-$ a species that provides Au^0, which is necessary for the nucleation and formation of nanoparticles (Equation 2). Therefore, the higher the concentration of $[AuCl_4]^-$ the more nuclei can be provided, contributing to a more significant number of nanoparticles[21]. Therefore, it is concluded that the most suitable concentration of $HAuCl_4$ in AuNPs-GAmb synthesis is 0.3 mM.

$$3Cit_{(red)} + [AuCl_4]^- \rightarrow 3Cit_{(oxi)} + Au^0 + 4Cl^- + 3CO_2 + 3H^+ \quad (2)$$

Once the best concentrations of GAmb (0.2%) and $HAuCl_4$ (0.3 mM), the influence of temperature and pH were studied. Figure 3A and 3B show the triplicates and averages of the absorption spectra recorded for the AuNPs-GAmb synthesized at temperatures of 80, 90, or 100 ºC. The results showed that increasing the temperature increased the nanoparticle formation rate, evidenced by the increasing absorbance values. A slight shift from 542 to 530 nm in the SPR band of the AuNPs-GAmb was obtained when the temperature varied from 80 to 90 or 100 ºC. This displacement may be related to an increase in the diameter of these nanoparticles since higher temperatures favor the formation of larger particles due to the increased supply of Au monomers[22].

Studies using Acacia and Xanthan gums showed that increasing the temperature in the reaction medium promoted an increase in the rate of AuNPs formation and improved the size distribution of the nanoparticles obtained. In the present study, GAmb was associated with the temperature of 100 °C and favored the more excellent formation of nanoparticles; the AuNPs-GAmb obtained at 100 °C presented the lowest polydispersity index (approximately 0.618), Table 1. Given the advantages observed when using the temperature of 100 °C, this was considered the optimal synthesis temperature.

The literature reports stated that pH between 2.8 and 4.0 is the most suitable for synthesizing gold nanoparticles, using $HAuCl_4$ as a precursor[23]. According to these studies, the initial amount of the $AuCl_4^-$ species available for forming AuNPs is directly related to the pH of the reaction medium.

The pH after the 0.2% GAmb and 0.3 mM $HAuCl_4$ mixture was 3.5. From small aliquots of 0.1 mol L^{-1} HCl, the pH value was adjusted to 3.0 and 2.5 to evaluate the effect of this parameter on AuNPs-GAmb properties. The UV-Vis spectra obtained in the syntheses of AuNPs-GAmb at these pHs are shown in Figure 3C and 3D, where it is

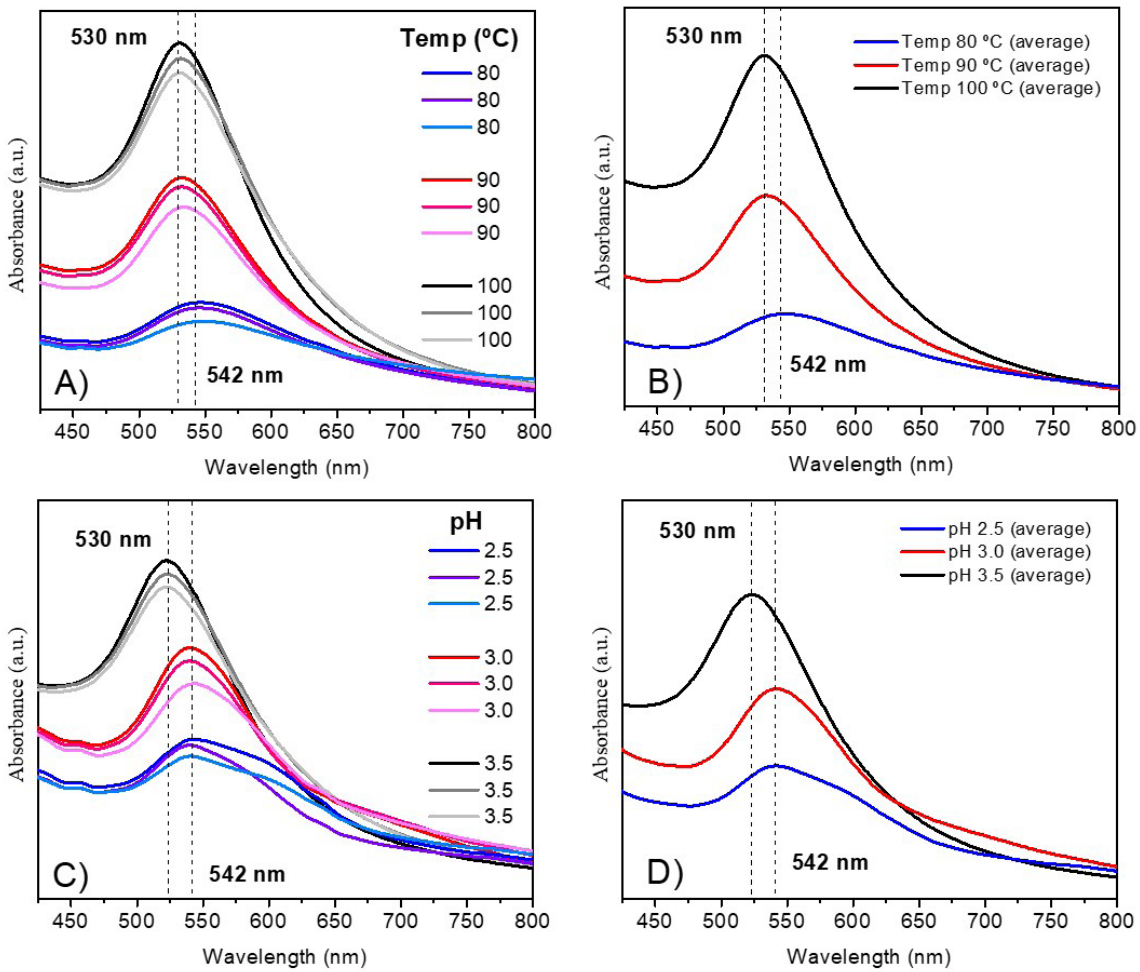

Figure 3. UV-Vis spectra (A) obtained in triplicate during the study of the temperature influence varied at 80, 90, or 100 ºC and (B) average of these triplicates. (C) UV-Vis obtained in triplicate during the pH study, and D) average of these triplicates. Constant parameters: GAmb concentration = 0.2%, $HAuCl_4$ concentration = 0.3 mM, and synthesis time = 30 min.

possible to observe that pH 3.5 promoted the formation of a more significant number of AuNPs-GAmb, in addition to the fact that at this pH the nanoparticles with smaller diameters (52.55 nm) and a higher zeta potential (-21.73 mV), suggesting better colloidal stability, Table 1. The results achieved in our study agree with previous studies, such as in the case of the synthesis of AuNPs using oats (*Avena sativa*) as a reducing and stabilizing agent, in which the pH of 3.5 was also considered an optimized condition[24]. Wuithschick et al.[25] affirmed that 2.8 is the minimum pH value adequate for synthesizing AuNPs from $HAuCl_4$ as a precursor salt.

The last optimized synthesis parameter was the reaction time. Thus, syntheses were performed at 30, 60, and 120 min, and the UV-Vis spectra obtained are shown in Figure 4A and 4B. After only 30 min of synthesis, it was already possible to observe a well-defined SPR band at around 530 nm for the AuNPs-GAmb. As the reaction time increased, there was an increase in the intensity of this band, indicating that the synthesis time promotes an increase in the formation of AuNPs-GAmb. The rise in synthesis time also influenced the size of the nanostructures formed, being 52.55 nm for 30 min, 32.39 nm for 60 min, and 26.50 nm for 120 min, Table 1. However, the increase in synthesis time promoted a decrease in the zeta potential value, being -21.73 mV for 30 min, -20.40 mV for 60 min, and -18.80 mV for 120 min. Thus, aiming for the practicality of the synthesis, 60 minutes was chosen as the optimal time for synthesizing AuNPs-GAmb.

The AuNPs-GAmb obtained under optimized conditions (0.2% Gamb, 0.3 mM $HAuCl_4$, temperature of 100 °C, pH 3.5, and time of 60 min) were very stable colloidal systems. After synthesizing the AuNPs-GAmb, they were stored, protected from light, and in a refrigerator for six months. They maintained their spectroscopic profile practically identical to that obtained approximately one hour after the synthesis (Figure 4C). The use of GAmb may explain the high stability of these nanostructures, as GAmb generates a steric barrier around these AuNPs and prevents them from aggregating.

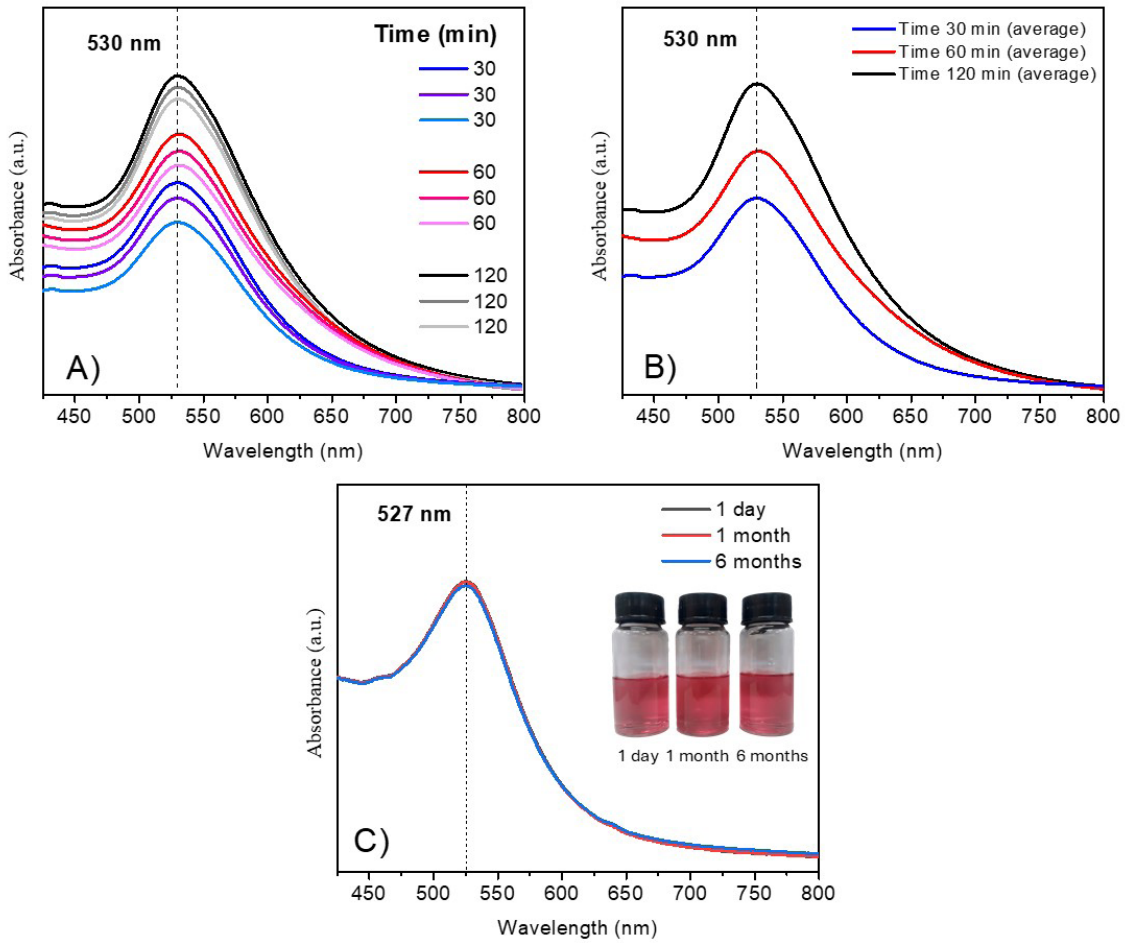

Figure 4. UV-Vis spectra (A) obtained in triplicate during the synthesis time study (30, 60 or 120 minutes) performed in triplicates and (B) average of these spectra. (C) Spectra obtained during the stability test of AuNPs-GAmb obtained one day, one month, and six months after synthesis. Constant parameters: GAmb concentration = 0.2%, $HAuCl_4$ concentration = 0.3 mM, pH = 3.5, and temperature = 100 °C.

3.3 Characterization by FTIR

Figure 5 shows the FTIR spectra recorded for GAmb and AuNPs-GAmb, with the leading bands at 3423, 2922, 1730, 1640, 1152, 1002, and 782 cm^{-1}. The broad band observed at 3423 cm^{-1} is attributed to the stretching vibrations of the –OH groups in GAmb. The band at 2922 cm^{-1} corresponds to the asymmetric stretching vibration of the methylene, methyl, and methoxy groups. The band at 1730 cm^{-1} can be attributed to carbonyl (C=O) stretching vibrations present in ketones, aldehydes, and carboxylic acids, which is the case of GAmb. The band observed at 1640 cm^{-1} corresponds to the asymmetric stretching of the carboxylate group (COO-), while the C–O stretching vibration of the ether and alcohol groups is confirmed at 1152 cm^{-1}. The intense band at 1002 cm^{-1} corresponds to the asymmetric stretching (C-O) bond present in esters and in the glycosidic bond of carbohydrates, as is the case of polysaccharides. The band at 782 cm^{-1} is associated with the stretching of the glycosidic bond present in carbohydrates[26].

In general, the FTIR spectrum of AuNPs-GAmb also showed the main characteristic peaks of GAmb, Figure 4. A change in intensity in the peaks of the FTIR spectrum of

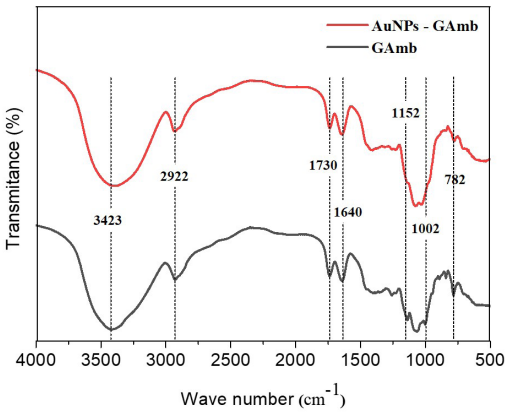

Figure 5. FTIR spectra of GAmb and AuNPs-GAmb.

AuNPs-GAmb was observed at 1152 and 1002 cm^{-1}, suggesting an interaction of AuNPs with carboxylate, acetyl and C-O groups of the ethers and alcohols present in the GAmb structure. Thus, FTIR studies suggest that the carbonyl and

hydroxyl groups have a greater affinity to bind to the metal[27], favoring the formation of a coating on the nanoparticles and increasing stabilization against accumulation.

3.4 Morphological characterization by AFM

AFM was used to characterize the size and shape of the AuNPs-GAmb (Figure 6A-E). In general, when measured by AFM, AuNPs-GAmb showed a spherical shape and an average diameter of 13.22 ± 1.86 nm. This diameter value has differed from that found for these nanostructures using the DLS technique (32.39 ± 0.801 nm). This disagreement was expected since the DLS technique measures the hydrodynamic diameter of the material; that is, in this measurement, both the metallic portion (AuNPs) and its polymeric shell (GAmb) are considered, thus providing information on the dimensions of the entire conjugate[28]. After optimizing the synthesis parameters, the nanoparticles presented a Zeta potential of –20.8 mV, indicating that GAmb, which has negatively charged groups, helps to stabilize the nanoparticle. In Figure 6C, both the metallic

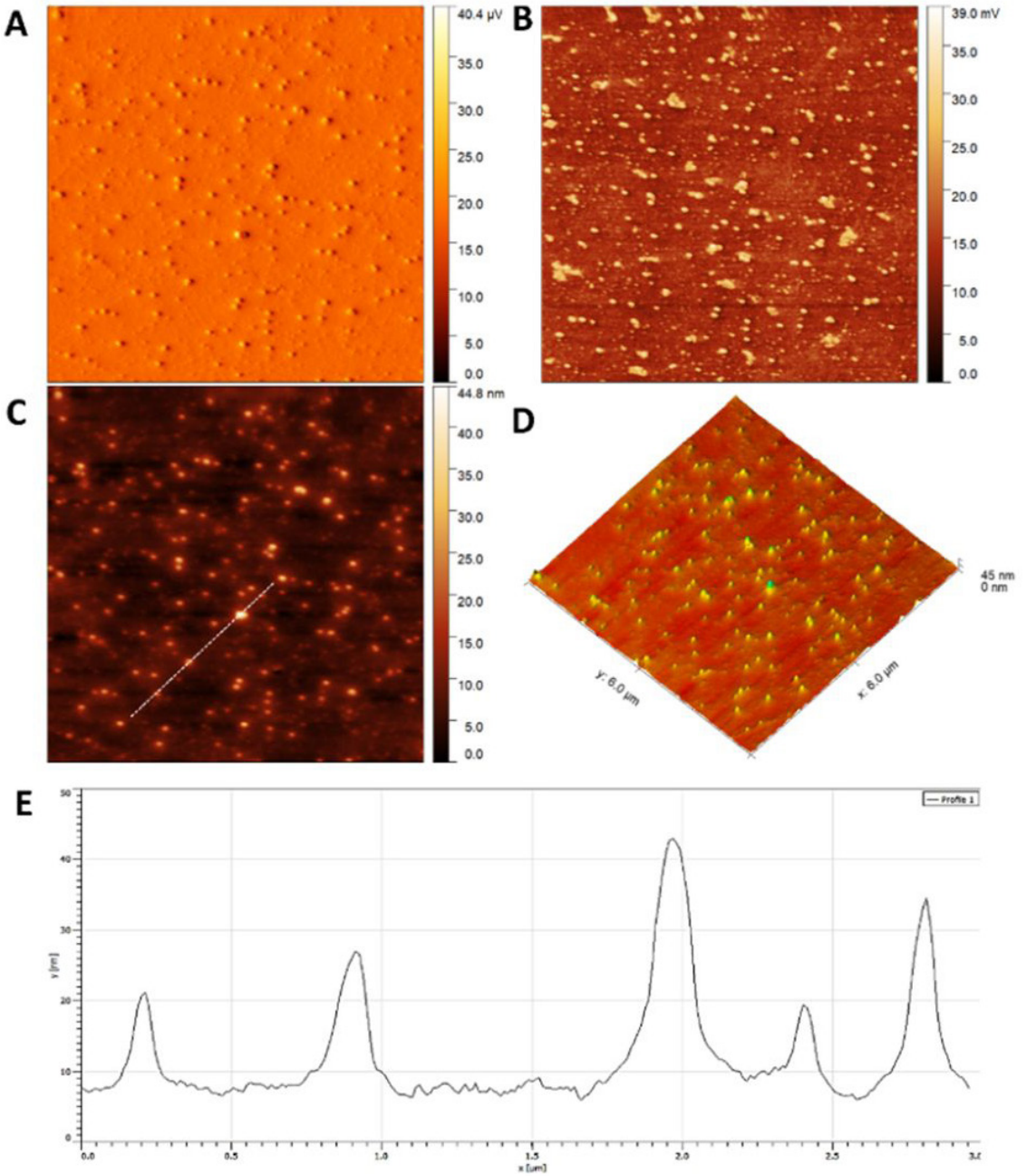

Figure 6. AFM images of AuNPs-GAmb. Amplitude (A), phase (B), 2D topography (C), 3D topography (D), and nanoparticle profile image (E). The profile was extracted along the white dotted line (in panel C). All images have 512 pixels resolution.

and polymeric portions that constitute the AuNPs-GAmb can be observed in detail.

3.5 AuNPs-GAmb in the catalytic degradation of dyes

Due to their minimal size and high surface area to volume ratio, metal nanoparticles can act as excellent catalysts in organic synthesis, reduction of pollutants such as 4-nitrophenol, and degradation of organic dyes[29]. Thus, we sought to evaluate the catalytic potential of AuNPs-GAmb against the reduction of methylene blue (MB), toluidine blue (TB), and methyl orange (MO). For comparative purposes, 0.03 M sodium borohydride ($NaBH_4$), a potent reducing agent, was used as a control during these experiments.

The pure aqueous solution of MB has a characteristic blue coloration with a maximum absorbance of 662 nm. When using 1.0 mL of $NaBH_4$ (0.03 mol L^{-1}) in the reduction of MB, only minor variations in its absorbance were observed, even after 120 minutes of the addition of $NaBH_4$, indicating that the reduction of MB with this compound is extremely slow, Figure 7A. On the other hand, after the addition of 100 µL of AuNPs-GAmb to the reaction medium, the characteristic absorption peak of MB disappeared in only 7 minutes, and the MB solution, previously an intense blue, became colorless, Figure 7B. The action of AuNPs-GAmb promoted the efficient catalysis of MB reduction to leucomethylene blue (LB), which is colorless and less toxic[30]. The correlations of the kinetics of this reaction are shown in Figure 7C.

Toluidine blue (TB) also has an intense blue coloration and a maximum absorption peak at 631 nm. Like MB, $NaBH_4$ promoted a slow reduction of TB, even after 120 minutes of action, Figure 7D. However, after adding 100 µL of the AuNPs-GAmb suspension, almost 100% of the dye degradation was observed 8 minutes later, Figure 6E. The correlations of the kinetics of this reaction are shown in Figure 07F. These results corroborate with the literature[31], which reported a time of 09 minutes for the catalytic degradation of MB using AuNPs reduced with the polysaccharide extracted from *Sargassum serratifolium*.

Methyl orange (MO) has an azo group (R-N = N-R') that acts as a chromophore, which gives the dye its orange color and absorbs in the 464 nm region. Figure 7G shows the UV-Vis absorption spectra for MO in the presence of $NaBH_4$ as a function of the action time. As was reported for the previous dyes, minor variations resulting from a slow degradation of MO by $NaBH_4$ were observed. On the other

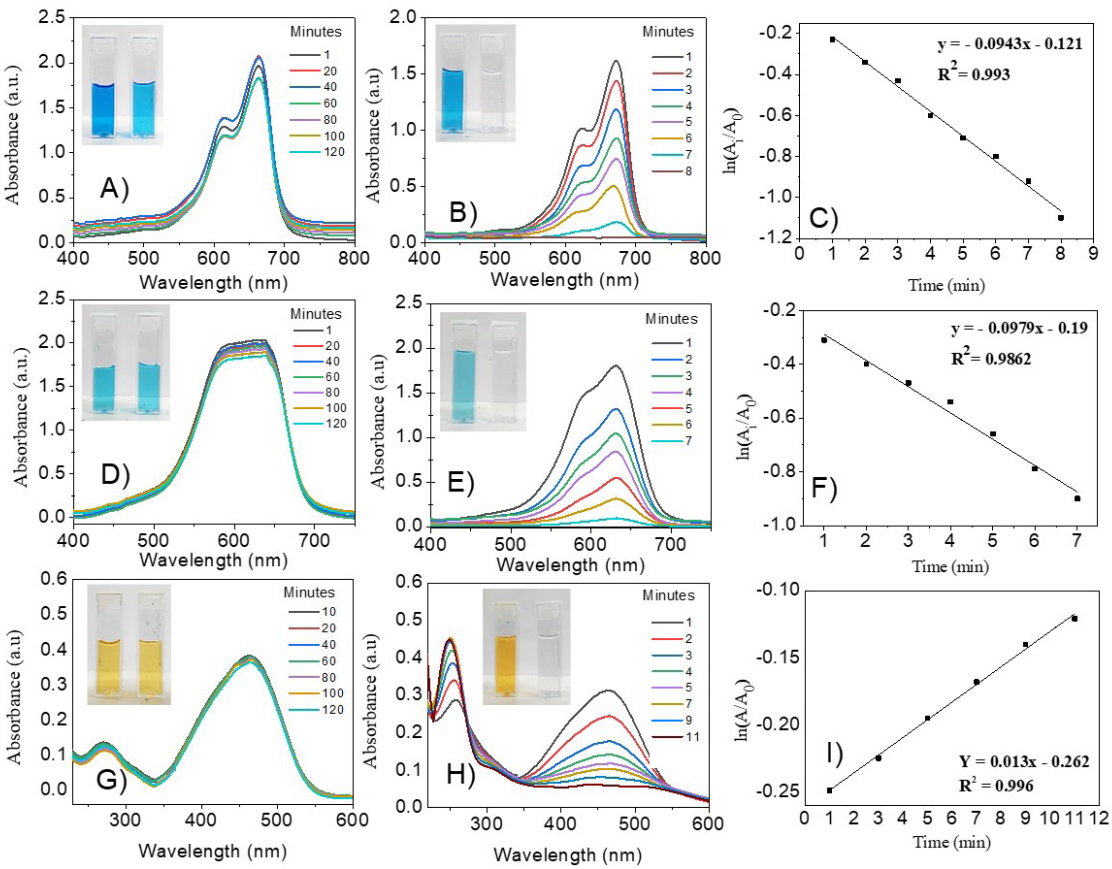

Figure 7. UV-Vis spectra showing the action of AuNPs-GAmb in the degradation of organic dyes. (A) MB + $NaBH_4$, (B) MB + $NaBH_4$ + AuNPs-GAmb, (C) Variation of MB absorbance *vs*. nanoparticles action time; (D) TB + $NaBH_4$, E) TB + $NaBH_4$ + AuNPs-GAmb, (F) Variation of TB absorbance *vs*. nanoparticles action time; (G) MO + $NaBH_4$, H) MO + $NaBH_4$ + AuNPs-GAmb, (I) Variation of MO absorbance *vs*. nanoparticles action time.

Table 2. Results of degradation time, kinetic constant, correlation coefficient and degradation percentage of TB, MB and MO.

Dyes	Reaction time (min)	K (min $^{-1}$)	Correlation coefficient (R^2)	% degradation
TB	8	0.098	0.986	97.100
MB	7	0.094	0.993	95.140
MO	11	0.013	0.996	84.300

hand, after only 11 minutes of adding 100 µL of AuNPs-GAmb to the medium containing the dye, the absorption band at 464 nm reduces considerably, suggesting a rapid degradation promoted by the presence of AuNPs-GAmb, Figure 7H. The MO degradation using AuNPs-GAmb as a catalyst was better than in other studies[32], which achieved a 20-minute degradation time with AuNPs reduced by *Persea americana* seeds.

Since the concentration of $NaBH_4$ used as a reductant in this study largely exceeds that of the dyes, the reaction rate is assumed to depend only on dye concentration. For this reason, the rate is assumed to be pseudo-first-order kinetics and can be denoted as:

$$ln[C]/[C_0]=-kt \quad (3)$$

Where:

[C] is the dye concentration at time t,

[C_0] is the initial concentration value.

Since absorbance is proportional to the solution concentration, the absorbance at time t (A) and time 0 (A_0) is comparable to the concentration at time t (C) and time 0 (C_0). The linear graphs of ln(A/A_0) versus time in both reactions confirmed that the reactions are by pseudo-first-order kinetics (Figure 7C, F, and I). The rate constant of each reaction calculated from the slope of the linear graph of ln(A/A_0) versus reaction time is detailed in Table 2. This table also shows the degradation efficiency of the dyes by the catalytic action of AuNPs-GAmb by calculating the % degradation.

In all degradation reactions, AuNPs-GAmb assumed the role of electron transfer mediators between the dye and $NaBH_4$, and the catalytic reduction proceeds by an electron relay effect[33]. As soon as the reagents are adsorbed on the surface of AuNPs-GAmb, the catalytic reaction occurs by electron transmission from BH_4- to the dyes, where the nanoparticles assist in the reduction reactions by decreasing the activation energy of these reactions, thus playing the role of an efficient catalyst.

3.6 ABTS radical scavenging activity

Antioxidants such as metallic nanoparticles inhibit oxidation, preventing the formation of free radicals or even eliminating and decomposing these species. Thus, the antioxidant activity of AuNPs-GAmb was evaluated by the $ABTS^{\bullet+}$ radical scavenging method. The stabilization of the $ABTS^{\bullet+}$ radical occurs through the oxidation reaction between the potassium persulfate salt (K_2SO_5) and the aqueous solution of $ABTS^{\bullet+}$. Thus, the antioxidant activity of AuNPs-GAmb is evaluated by discoloration of the $ABTS^{\bullet+}$ radical solution, with the data denoted as the percentage of inhibition of this radical, Figure 8. This study found that AuNPs-GAmb were responsible for inhibiting the $ABTS^{\bullet+}$ radical in a concentration-dependent manner. The IC_{50} obtained for AuNPs-GAmb was 0.63 ± 0.11 mg mL^{-1}. These results are close to those obtained in other studies involving the antioxidant activity of AuNPs stabilized with natural polymers[34].

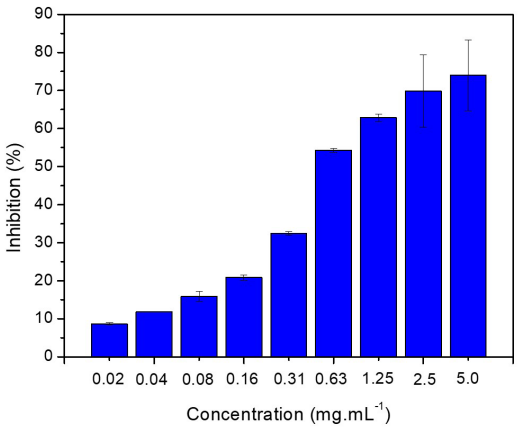

Figure 8. Percentage inhibition of the $ABTS^{\bullet+}$ radical by AuNPs-GAmb.

4. Conclusions

In this study, a route for the green synthesis of gold nanoparticles reduced and stabilized with *Amburana cearensis* gum (AuNPs-GAmb) was proposed for the first time. Under the optimized conditions, spherical AuNPs-GAmb with a diameter of 13.22 ± 1.86 nm were obtained. AuNPs-GAmb played an efficient role as catalysts in the degradation of harmful dyes, inactivating dyes such as toluidine blue, methylene blue, and methyl orange in less than 11 minutes. In addition, AuNPs-GAmb also showed antioxidant activity against $ABTS^{\bullet+}$ radical, with IC50 of 0.63 ± 0.11 mg mL^{-1}. Thus, AuNPs-GAmb are promising, low-cost, and practical green materials for biotechnological applications.

5. Author's Contribution

- **Conceptualization –** Eziel Cardoso da Silva; Emanuel Airton de Oliveira Farias; Thais Danyelle Santos Araújo; Alyne Rodrigues Araújo; Lívio César Cunha Nunes; Carla Eiras.
- **Data curation –** Eziel Cardoso da Silva; Carla Eiras.
- **Formal analysis –** Eziel Cardoso da Silva; Carla Eiras.
- **Funding acquisition –** Carla Eiras.
- **Investigation –** Eziel Cardoso da Silva; Emanuel Airton de Oliveira Farias; Thais Danyelle Santos Araújo; Alyne

Rodrigues Araújo; Lívio César Cunha Nunes; Carla Eiras.

- **Methodology –** Thais Danyelle Santos Araújo; Alyne Rodrigues Araújo; Carla Eiras.
- **Project administration –** Lívio César Cunha Nunes; Carla Eiras.
- **Resources –** NA.
- **Software –** NA.
- **Supervision –** Carla Eiras; Emanuel Airton de Oliveira Farias.
- **Validation –** Carla Eiras; Emanuel Airton de Oliveira Farias; Lívio César Cunha Nunes.
- **Visualization –** Carla Eiras; Emanuel Airton de Oliveira Farias; Lívio César Cunha Nunes.
- **Writing – original draft –** Carla Eiras; Eziel Cardoso da Silva.
- **Writing – review & editing –** Carla Eiras; Geanderson Emilio de Almeida; Eziel Cardoso da Silva.

6. Acknowledgements

This work received financial support from CNPq (Process: 310764/2023-8) and INCT iCEIS (process: 406264/2022-8) and FAPEPI/CNPq (process: 00110.000202 /2022-28).

7. References

1. Gómez-López, P., Puente-Santiago, A., Castro-Beltrán, A., do Nascimento, L. A. S., Balu, A. M., Luque, R., & Alvarado-Beltrán, C. G. (2020). Nanomaterials and catalysis for green chemistry. *Current Opinion in Green and Sustainable Chemistry*, *24*, 48-55. http://doi.org/10.1016/j.cogsc.2020.03.001.
2. Li, R., Chen, X., Ye, H., & Sheng, X. (2024). Green synthesis of gold nanoparticles from the extract of *Crocus sativus* to study the effect of antidepressant in adolescence and to observe its aggressive and impulsive behavior in rat models. *South African Journal of Botany*, *165*, 455-465. http://doi.org/10.1016/j.sajb.2023.12.029.
3. Younis, H. M., Hussein, H. A., Khaphi, F. L., & Saeed, Z. K. (2023). Green biosynthesis of silver and gold nanoparticles using Teak (*Tectona grandis*) leaf extract and its anticancer and antimicrobial activity. *Heliyon*, *9*(11), e21698. http://doi.org/10.1016/j.heliyon.2023.e21698. PMid:38027825.
4. Veras, B. O., Moura, G. M. M., Barros, A. V., Silva, M. V., Assis, P. A. C., Aguiar, J. C. R. O. F., Navarro, D. M. A. F., Ximenes, R. M., Wanderley, A. G., Oliveira, M. B. M., & Lopes, A. C. S. (2023). Antinociceptive and anti-inflammatory activities of essential oil of the leaves of *Amburana cearensis* (Allemão) A.C. Smith. from the semi-arid region of Northeastern Brazil. *Journal of Ethnopharmacology*, *317*, 116858. http://doi.org/10.1016/j.jep.2023.116858. PMid:37400005.
5. Venkatesan, D., Umasankar, S., Mangesh, V. L., Krishnan, P. S., Tamizhdurai, P., Kumaran, R., & Baskaralingam, P. (2023). Removal of Toluidine blue in water using green synthesized nanomaterials. *South African Journal of Chemical Engineering*, *45*, 42-50. http://doi.org/10.1016/j.sajce.2023.04.006.
6. Jayamohan, H., Smith, Y. R., Gale, B. K., Mohanty, S. K., & Misra, M. (2016). Photocatalytic microfluidic reactors utilizing titania nanotubes on titanium mesh for degradation of organic and biological contaminants. *Journal of Environmental Chemical Engineering*, *4*(1), 657-663. http://doi.org/10.1016/j.jece.2015.12.018.
7. Deokar, G. K., & Ingale, A. G. (2023). Exploring effective catalytic degradation of organic pollutant dyes using environment benign, green engineered gold nanoparticles. *Inorganic Chemistry Communications*, *151*, 110649. http://doi.org/10.1016/j.inoche.2023.110649.
8. Farias, E. A. O., Almeida, G. E., Araújo, I. C., Araujo-Nobre, A. R., Furtado, N. J. S., Nunes, L. C. C., & Eiras, C. (2024). Screen-printed electrode modified with a composite based on *Amburana cearensis* gum, multi-walled carbon nanotubes, and gold nanoparticles for electrochemical determination of total isoflavones in soybean cultivars. *Journal of Solid State Electrochemistry*, *29*(3), 1121-1137. http://doi.org/10.1007/s10008-024-05963-x.
9. Melo, M. A., Jr., Santos, L. S. S., Gonçalves, M. C., & Nogueira, A. F. (2012). Preparação de nanopartículas de prata e ouro: um método simples para introduzir a nanotecnologia em laboratórios de ensino. *Quimica Nova*, *35*(9), 1872-1878. http://doi.org/10.1590/S0100-40422012000900030.
10. Silva, A. A. (2016). *Síntese e estabilização de nanopartículas de ouro para fins biotecnológicos e cosméticos* (Master's thesis). Universidade de São Paulo, São Paulo.
11. Queen, J. E., Prasad, T. A. A., Vithiya, B. S. M., Odhah, O. H., Kumar, N. S., Tamizhdurai, P., Alreshaidan, S. B., Basivi, P. K., Pabba, D. P., & Al-Fatesh, A. S. (2025). Optimized green synthesis of gold nanoparticles from cranberry fruit extract using response surface methodology for enhanced biomedical applications and catalytic degradation. *Bioorganic Chemistry*, *161*, 108546. http://doi.org/10.1016/j.bioorg.2025.108546. PMid:40334423.
12. Princy, K. F., & Gopinath, A. (2018). Optimization of physicochemical parameters in the biofabrication of gold nanoparticles using marine macroalgae *Padina tetrastromatica* and its catalytic efficacy in the degradation of organic dyes. *Journal of Nanostructure in Chemistry*, *8*(3), 333-342. http://doi.org/10.1007/s40097-018-0277-2.
13. Bogireddy, N. K. R., & Agarwal, L. V. (2019). *Persea americana* seed extract mediated gold nanoparticles for mercury(II)/iron(III) sensing, 4-nitrophenol reduction, and organic dye degradation. *RSC Advances*, *9*(68), 39834-39842. http://doi.org/10.1039/C9RA08233F. PMid:35541370.
14. Gião, M. S., González-Sanjosé, M. L., Rivero-Pérez, M. D., Pereira, C. I., Pintado, M. E., & Malcata, F. X. (2007). Infusions of Portuguese medicinal plants: dependence of final antioxidant capacity and phenol content on extraction features. *Journal of the Science of Food and Agriculture*, *87*(14), 2638-2647. http://doi.org/10.1002/jsfa.3023. PMid:20836172.
15. Silva, J. R. T., Araújo, I. C., Silva, E. C., Santana, M. V., Almeida, G. E., Farias, E. A. O., Lima, L. R. M., Paula, R. C. M., Silva, D. A., Araújo, A. R., & Eiras, C. (2024). Polysaccharide from Cumaru (Amburana cearensis) exudate and its potential for biotechnological applications. *Polímeros: Ciência e Tecnologia*, *34*(1), e20240008. https://doi.org/10.1590/0104-1428.20230025.
16. Tessema, B., Gonfa, G., Hailegiorgis, S. M., Prabhu, S. V., & Manivannan, S. (2023). Synthesis and characterization of silver nanoparticles using reducing agents of bitter leaf (*Vernonia amygdalina*) extract and tri-sodium citrate. *Nano-Structures & Nano-Objects*, *35*, 100983. http://doi.org/10.1016/j.nanoso.2023.100983.
17. Chopra, H., Bibi, S., Singh, I., Hasan, M. M., Khan, M. S., Yousafi, Q., Baig, A. A., Rahman, M. M., Islam, F., Emran, T. B., & Cavalu, S. (2022). Green metallic nanoparticles: biosynthesis to applications. *Frontiers in Bioengineering and Biotechnology*, *10*, 874742. http://doi.org/10.3389/fbioe.2022.874742. PMid:35464722.
18. Kumar, S., Gandhi, K. S., & Kumar, R. (2007). Modeling of formation of gold nanoparticles by citrate method. *Industrial*

& Engineering Chemistry Research, *46*(10), 3128-3136. http://doi.org/10.1021/ie060672j.

19. Ji, X., Song, X., Li, J., Bai, Y., Yang, W., & Peng, X. (2007). Size control of gold nanocrystals in citrate reduction: the third role of citrate. *Journal of the American Chemical Society*, *129*(45), 13939-13948. http://doi.org/10.1021/ja074447k. PMid:17948996.
20. Al-Radadi, N. S., Al-Bishri, W. M., Salem, N. A., & ElShebiney, S. A. (2024). Plant-mediated green synthesis of gold nanoparticles using an aqueous extract of *Passiflora ligularis*, optimization, characterizations, and their neuroprotective effect on propionic acid-induced autism in Wistar rats. *Saudi Pharmaceutical Journal*, *32*(2), 101921. http://doi.org/10.1016/j.jsps.2023.101921. PMid:38283153.
21. Ghosh, S., Patil, S., Ahire, M., Kitture, R., Jabgunde, A., Kale, S., Pardesi, K., Bellare, J., Dhavale, D. D., & Chopade, B. A. (2011). Synthesis of gold nanoanisotrops using *Dioscorea bulbifera* tuber extract. *Journal of Nanomaterials*, *1*, 354793. http://doi.org/10.1155/2011/354793.
22. Mohammadi, F. M., & Ghasemi, N. (2018). Influence of temperature and concentration on biosynthesis and characterization of zinc oxide nanoparticles using cherry extract. *Journal of Nanostructure in Chemistry*, *8*(1), 93-102. http://doi.org/10.1007/s40097-018-0257-6.
23. Babaei, Z., Majidi, R. F., Negahdari, B., & Tavoosidana, G. (2018). 'Inversed Turkevich' method for tuning the size of gold nanoparticles: evaluation the effect of concentration and temperature. *Nanomedicine Research Journal*, *3*(4), 190-196. http://doi.org/10.22034/nmrj.2018.04.003.
24. Armendariz, V., Herrera, I., Peralta-Videa, J. R., Jose-Yacaman, M., Troiani, H., Santiago, P., & Gardea-Torresdey, J. L. (2004). Size controlled gold nanoparticle formation by *Avena sativa* biomass: use of plants in nanobiotechnology. *Journal of Nanoparticle Research*, *6*(4), 377-382. http://doi.org/10.1007/s11051-004-0741-4.
25. Wuithschick, M., Birnbaum, A., Witte, S., Sztucki, M., Vainio, U., Pinna, N., Rademann, K., Emmerling, F., Kraehnert, R., & Polte, J. (2015). Turkevich in new robes: key questions answered for the most common gold nanoparticle synthesis. *ACS Nano*, *9*(7), 7052-7071. http://doi.org/10.1021/acsnano.5b01579. PMid:26147899.
26. Liu, H., Zhang, M., Meng, F., Wubuli, A., Li, S., Xiao, S., Gu, L., & Li, J. (2024). HAuCl4-mediated green synthesis of highly stable Au NPs from natural active polysaccharides: synthetic mechanism and antioxidant property. *International Journal of Biological Macromolecules*, *265*(Pt 2), 130824. http://doi.org/10.1016/j.ijbiomac.2024.130824. PMid:38492708.
27. Liu, H., Zhang, M., Meng, F., Su, C., & Li, J. (2023). Polysaccharide-based gold nanomaterials: synthesis mechanism, polysaccharide structure-effect, and anticancer activity. *Carbohydrate Polymers*, *321*, 121284. http://doi.org/10.1016/j.carbpol.2023.121284. PMid:37739497.
28. Bhattacharjee, S. (2016). DLS and zeta potential – What they are and what they are not? *Journal of Controlled Release*, *235*, 337-351. http://doi.org/10.1016/j.jconrel.2016.06.017. PMid:27297779.
29. Karami, S., Esfahani, F. E., & Karimi, B. (2023). Gold nanoparticles supported on carbon-coated magnetic nanoparticles: A robust and effective catalyst for aerobic alcohols oxidation in water. *Molecular Catalysis*, *534*, 112772. http://doi.org/10.1016/j.mcat.2022.112772.
30. Shahzaib, A., Shaily, Ahmad, I., Alshehri, S. M., Ahamad, T., & Nishat, N. (2024). Green synthesis of ZIF-67 composite embedded with magnetic nanoparticles and ZnO decoration for efficient catalytic reduction of rhodamine B and methylene blue. *Chemistry of Inorganic Materials*, *2*, 100037. http://doi.org/10.1016/j.cinorg.2024.100037.
31. Kim, B., Song, W. C., Park, S. Y., & Park, G. (2021). Green synthesis of silver and gold nanoparticles via *Sargassum serratifolium* extract for catalytic reduction of organic dyes. *Catalysts*, *11*(3), 347. http://doi.org/10.3390/catal11030347.
32. Reddy, G. B., Madhusudhan, A., Ramakrishna, D., Ayodhya, D., Venkatesham, M., & Veerabhadram, G. (2015). Green chemistry approach for the synthesis of gold nanoparticles with gum kondagogu: characterization, catalytic and antibacterial activity. *Journal of Nanostructure in Chemistry*, *5*(2), 185-193. http://doi.org/10.1007/s40097-015-0149-y.
33. Memon, K., Memon, R., Khalid, A., Al-Anzi, B. S., Uddin, S., Sherazi, S. T. H., Chandio, A., Talpur, F. N., Latiff, A. A., & Liaqat, I. (2023). Synthesis of PVP-capped trimetallic nanoparticles and their efficient catalytic degradation of organic dyes. *RSC Advances*, *13*(42), 29272-29282. http://doi.org/10.1039/D3RA03663D. PMid:37818256.
34. Padalia, H., & Chanda, S. (2021). Antioxidant and anticancer activities of gold nanoparticles synthesized using aqueous leaf extract of *Ziziphus nummularia*. *BioNanoScience*, *11*(2), 281-294. http://doi.org/10.1007/s12668-021-00849-y.

Received: Nov. 25, 2024
Revised: Mar. 18, 2025
Accepted: May 12, 2025

Editor-in-Chief: Sebastião V. Canevarolo